

Ab initio calculations for bromine adlayers on the Ag(100) and Au(100) surfaces: the $c(2 \times 2)$ structure

Sanwu Wang¹ and Per Arne Rikvold^{1,2}

¹*School of Computational Science and Information Technology,
and Center for Materials Research and Technology,
Florida State University, Tallahassee, Florida 32306-4120*

²*Department of Physics, Florida State University, Tallahassee, Florida 32306-4350*

Ab initio total-energy density-functional methods with supercell models have been employed to calculate the $c(2 \times 2)$ structure of the Br-adsorbed Ag(100) and Au(100) surfaces. The atomic geometries of the surfaces and the preferred bonding sites of the bromine have been determined. The bonding character of bromine with the substrates has also been studied by analyzing the electronic density of states and the charge transfer. The calculations show that while the four-fold hollow-site configuration is more stable than the two-fold bridge-site topology on the Ag(100) surface, bromine prefers the bridge site on the Au(100) surface. The one-fold on-top configuration is the least stable configuration on both surfaces. It is also observed that the second layer of the Ag substrate undergoes a small buckling as a consequence of the adsorption of Br. Our results provide a theoretical explanation for the experimental observations that the adsorption of bromine on the Ag(100) and Au(100) surfaces results in different bonding configurations.

PACS numbers: 68.43.Bc, 68.43.Fg, 68.47.-b, 82.45.-h

I. INTRODUCTION

Anion adsorption on metals can strongly modify surface morphology and electronic structure and chemical reactivity. It is therefore of great scientific and technological importance. In particular, the halide-adsorbed noble-metal systems play a significant role in electrochemistry. From the fundamental point of view, halide-adsorbed noble-metal surfaces are important model systems for adsorption on metal surfaces with formation of ordered two-dimensional adsorbate structures. It is thus not surprising that the adsorption of halides on noble metals has been extensively investigated.

The systems we selected to study are the Br-chemisorbed Ag(100) and Au(100) surfaces. The adsorption of bromine on the Ag(100) and Au(100) surfaces both in vacuum and in solution have been widely studied by experiments¹⁻¹² and by classical simulations.¹³⁻¹⁶ Experimentally, bromine has been found to form different bonding structures on the Ag(100) and Au(100) surfaces. While bromine chemisorbed on the Ag(100) surface occupies the four-fold hollow site (hereafter referred to as H_4), the most stable chemisorption structure on Au(100) is the configuration with bromine at the two-fold bridge site (hereafter referred to as B_2). These different chemisorption structures have been verified by various experimental measurements.^{1-4,6-12} However, theoretical studies have not yet reproduced these different adsorption behaviors.

Kleinherbers *et al.* performed angle-resolved photoemission, low-energy electron diffraction (LEED), and X-ray photoemission measurements for the interaction of halides with Ag surfaces.¹ They found that the adsorption of Cl, Br, and I on the Ag(100) surface in vacuum all resulted in the formation of a $c(2 \times 2)$ overlayer with the adsorbates in the H_4 sites. Using *in situ* surface X-ray

scattering, Ocko *et al.* studied the adsorption of bromide on an Ag(100) electrode. They observed a disordered phase at lower coverages and an ordered $c(2 \times 2)$ phase at a coverage of half a monolayer.² The Br was determined to bond at the H_4 site in both the $c(2 \times 2)$ and disordered phases. The atomic geometry of the Br/Ag(100)- $c(2 \times 2)$ surface was further investigated by Endo *et al.* with the *in situ* X-ray absorption fine structure (XAFS) method.⁴ The H_4 site was confirmed to be the bonding site of bromine. The disordered phase of the Br/Ag(100) surface at lower bromine coverages was also recently further investigated experimentally.³ In that study, it was suggested that while most of the bromide ions occupy the H_4 sites, there are additional bromide ions adsorbed slightly off the H_4 sites.

The LEED data reported by Bertel *et al.*^{6,7} have shown that the chemisorption of Br on the Au(100) surface in vacuum results in the rearrangement of the top-layer Au atoms of the original clean reconstructed Au(100)-(5 \times 20) surface and the formation of an unreconstructed (1 \times 1) substrate structure. Several ordered structures of the Br adlayer, including $c(2 \times 2)$, $(\sqrt{2} \times 4\sqrt{2})R45^\circ$, and $c(4 \times 2)R45^\circ$, were obtained after bromine exposure on Au(100) surfaces, with the former two structures being metastable. It was concluded from the experimental data that Br adsorbed at the B_2 site on the Au(100) surface in all the observed phases. This is in contrast to the case of the Br-adsorbed Ag(100) surface. Under electrochemical *in situ* conditions, surface X-ray scattering and scanning tunneling microscopy (STM) experiments showed that bromide adsorbed on the unreconstructed Au(100)-(1 \times 1) surface forms a commensurate $c(\sqrt{2} \times 2\sqrt{2})R45^\circ$ structure and an incommensurate $c(\sqrt{2} \times 2p)R45^\circ$ ($p \leq 2\sqrt{2}$, depending on the applied potential).^{8,9,11,12} In this case, too, the bromide ions were determined to reside at the

B_2 sites.

In contrast to the considerable progress of the experimental measurements, theoretical studies employing *ab initio* methods to these systems are still at an early stage. Several groups have performed *ab initio* Hartree-Fock (HF) and density-functional-theory (DFT) calculations for the Br/Ag(100) and Br/Au(100) interfaces using cluster models.^{17–20} While these investigations have provided useful information about the interaction between Br and the surfaces, as we discuss below, many of the results are not yet sufficiently accurate. For example, the preferred bonding site of Br on the Au(100) surface was incorrectly predicted by *ab initio* DFT cluster calculations, which showed that Br would prefer to bond at the H_4 site on both the Ag(100) and Au(100) surfaces.¹⁸ Similarly, *ab initio* HF studies with small clusters predicted the bridge site as the preferred adsorption site for Br on Ag(100).¹⁹ Given that these calculations with small clusters cannot reproduce such a fundamental property as the binding site, all other results (*e.g.*, energy barriers) obtained from such calculations for both the Br/Ag(100) and Br/Au(100) systems are questionable.

Here we present results of total-energy DFT calculations in which we used supercell models for the Ag(100) and Au(100) surfaces. The detailed atomic structures and electronic properties of the chemisorbed surfaces and the preferred bonding site of the adsorbate have been determined. Our theoretical approach has reproduced the different behavior of Br on the Ag(100) and Au(100) surfaces. The most stable adsorption sites for Br chemisorbed on the Ag(100) and Au(100) surfaces are determined by our calculations to be the H_4 and the B_2 sites, respectively. Our results are in excellent agreement with the experimental data. The obtained results for the electronic properties also enable us to analyze the nature of the bonding between Br and the substrates and understand the different adsorption behavior of Br on the Ag(100) and Au(100) surfaces.

The remainder of this paper is organized as follows. In Sec. II we outline in detail the computational method and the supercell models that we used. In Sec. III we present and discuss the results for bulk, clean surfaces (Sec. III A), and adsorbed surfaces (Sec. III B). The adsorption geometries and atomic relaxations are discussed in Sec. III B1, and the electronic properties and bonding character in Sec. III B2. We also give comparisons of our results with previous calculations and experimental data. Finally, in Sec. IV, we summarize the main results of our calculations.

II. METHOD AND MODEL

On the Ag(100) and Au(100) surfaces, there are three different symmetric adsorption sites, known as H_4 , B_2 , and T_1 (on-top) sites. These three sites are shown in Fig. 1. We have studied a $c(2 \times 2)$ structure in which Br

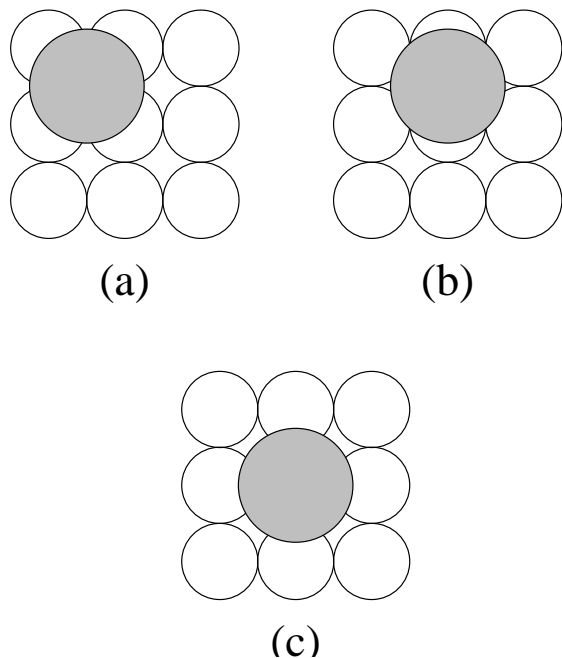


FIG. 1. Schematics of an adatom at (a) the four-fold hollow (H_4) site, (b) the two-fold bridge (B_2) site, and (c) the on-top (T_1) site on the unreconstructed Ag(100) and Au(100) surfaces.

forms an adlayer with a coverage of $\frac{1}{2}$ monolayer on the surface for each of the three bonding configurations.

The metal surface is modeled by repeated slabs with five, seven, and nine metal layers separated by a vacuum region equivalent to five or seven metal layers. Each metal layer in the supercell contains two metal atoms. Br is adsorbed symmetrically on both sides of the slab. All the metal atoms were initially located at their bulk positions, with the equilibrium lattice constant of the bulk determined by our calculations.

The calculations were performed within density-functional theory, using the pseudopotential (PP) method and a plane-wave basis set. The results reported in this paper were obtained using the Vienna *ab-initio* simulation package (VASP).^{21–23} The exchange-correlation effects were treated with the generalized gradient-corrected exchange-correlation functionals (GGA) given by Perdew and Wang.^{24,25} We adopted the scalar-relativistic Vanderbilt ultrasoft pseudopotentials supplied by Kresse and Hafner^{26,27}. A plane-wave energy cutoff of 20 Ry and 56 special \mathbf{k} points in the irreducible part of the two-dimensional Brillouin zone of the $c(2 \times 2)$ surface were used for calculating both the Br/Ag(100) and Br/Au(100) surfaces. Optimization of the atomic structure was performed for each supercell *via* a conjugate-gradient technique using the total energy and the Hellmann-Feynman forces on the atoms.²⁸ All the structures were fully relaxed until the change in total energy was smaller than 1 meV between two ionic steps. The convergence of the total energies was checked with

different values of the plane-wave cutoff and different numbers of special \mathbf{k} points. A series of test calculations with different slab thicknesses (from five to nine metal layers) and vacuum-gap widths (equivalent to five and seven metal layers) were also carried out to check convergence. The calculations on which this paper is based represent approximately 300 CPU hours on an IBM SP2 computer.

III. RESULTS AND DISCUSSION

A. Bulk and clean surface

We first present the calculated properties for bulk silver and bulk gold, and the relaxed but unreconstructed clean Ag(100) and Au(100) surfaces.

Calculations for bulk Ag and Au were conducted with 408 special \mathbf{k} points and cutoff energies ranging from 20 Ry to 40 Ry. The total energy convergence with respect to the cutoff energy was shown to be within a few tenths of 1 meV. We obtained lattice constants of 4.17 Å and 4.18 Å for bulk Ag and Au, about 2.0% and 2.5% larger than the corresponding experimental values²⁹ at room temperature, respectively. Previous total-energy DFT calculations at the GGA level found lattice constants between 4.13 Å and 4.19 Å for bulk Ag,^{30–37} and between 4.19 Å [Ref. 38] and 4.20 Å [Ref. 37] for bulk Au. Our results are in good agreement with these calculations.

The properties of the clean Ag(100) and Au(100) surfaces were calculated using supercells containing a 7-layer metal slab and a vacuum gap equivalent to 7 bulk-metal layers. A 1×1 surface cell was used with 66 special \mathbf{k} points in the surface Brillouin zone. The kinetic energy cutoff for the calculations was 20 Ry. All the layers except for the central one were relaxed. Surface reconstruction was not considered.

The surface energies for the Ag(100) and Au(100) surfaces obtained from our calculations are 0.43 eV/atom and 0.47 eV/atom, respectively. Both results are in good agreement with recent pseudopotential GGA calculations by Yu and Scheffler, who reported the corresponding values of 0.48 and 0.45 eV/atom.^{31,38} A recent calculation with linear-muffin-tin-orbital (LMTO)-GGA methods, however, obtained much larger values of 0.65 and 0.90 eV/atom for the unrelaxed Ag(100) and Au(100) surfaces, respectively.³⁷ The reason for the large discrepancy from the other GGA results is not clear. Pseudopotential local-density approximation (LDA),^{31,38} LMTO-LDA,^{39–41} and linearized augmented-plane-wave LDA^{42–44} calculations have provided values of 0.59–0.7 eV/atom, and 0.69–0.72 eV/atom for the surface energies of the Ag(100) and Au(100) surfaces, respectively. These DFT-LDA values for the surface energy are generally larger than those calculated with the DFT-GGA calculations reported in this paper and Refs. 31 and 38. This is consistent with the previous observation²⁴ that

LDA surface energies are normally larger than the corresponding GGA values due to the different treatment of the exchange-correlation functional. The calculated values for the surface energies are thus seen to be quite sensitive to the computational method and the form of the exchange-correlation functional.

Table I shows the results of the surface relaxation. While no significant structural relaxation is found for either surface, the Ag(100) surface shows a slightly more relaxed geometry than the Au(100) surface. Both surfaces show an inward relaxation of the top layer and slight outward relaxation of the second and third layers. LEED measurements⁴⁶ showed insignificant relaxation of the Ag(100) surface with $\Delta d_{12}/d_0 = 0 \pm 1.5\%$ and $\Delta d_{23}/d_0 = 0 \pm 1.5\%$, where Δd_{12} and Δd_{23} are the changes in spacing between the top and the second layer and between the second and the third layer, and d_0 is the bulk interlayer distance. Our results are thus in good agreement with the experimental data, and basically consistent with other *ab initio* calculations, the results of which are also listed in Table I for comparison.

B. Br-adsorbed Ag(100) and Au(100) surfaces

1. Relaxations and energetics

The results of our calculations for the Br/Ag(100)- $c(2 \times 2)$ and the Br/Au(100)- $c(2 \times 2)$ surfaces are shown in Tables II and III. If not otherwise indicated, the results reported in this section (and in Tables II and III) were calculated with a cutoff energy of 20 Ry, 56 special \mathbf{k} points, and supercells containing a 9-layer metal slab with a vacuum region equivalent to seven metal layers.

TABLE I. Relaxation of the clean Ag(100) and Au(100) surfaces. Δd_{ij} is the change of the interlayer distance, and d_0 is the corresponding distance in the bulk.

	$\Delta d_{12}/d_0$ (%)	$\Delta d_{23}/d_0$ (%)	$\Delta d_{34}/d_0$ (%)
Ag(100)			
This work	-1.8	0.7	0.2
PP-GGA ^a	-1.4		
PP-LDA ^a	-2.2	0.4	
PP-LDA ^b	-1.3	1.0	0.8
LMTO-LDA ^c	-1.9		
Experiment ^d	0 ± 1.5	0 ± 1.5	
Au(100)			
This work	-1.3	0.3	0.2
PP-LDA ^e	-1.2	0.4	
LMTO-LDA ^f	-1.0		

^aRef. 31.

^bRef. 45.

^cRefs. 39–41.

^dRef. 46.

^eRef. 38.

^fRefs. 40,41.

In-plane relaxations of the top-layer metal atoms were found to result in changes of the distance between Br and its nearest-neighbor metal atoms and of the total-energy difference between two different configurations within only 0.01 Å and a few meV, respectively. The effects of in-plane relaxations are thus negligible, and such relaxations were not considered in the calculations for the Br-adsorbed surfaces.

Table II shows total-energy differences between different bonding configurations of both surfaces. Each structure was optimized. We found that while the total energy of the H_4 configuration is lower by 213 meV than the B_2 configuration for the Br/Ag(100) surface, it is higher by 58 meV for the Br/Au(100) surface. The T_1 configuration for both surfaces is found to be higher in total energy than both the corresponding H_4 and B_2 configurations. Thus, we conclude that while Br adsorbed on the Ag(100) surface prefers the H_4 site, it is adsorbed at the B_2 site on the Au(100) surface. This conclusion is in agreement with experimental observations.^{1-4,6-12}

It is interesting to note that the magnitude of the total-energy difference between the H_4 and B_2 structures for Br/Ag(100) is significantly larger than the corresponding value for the Br/Au(100) surface. This suggests that diffusion of Br on the Au(100) surface may occur much more easily than on the Ag(100) surface since the total-energy difference between the most stable configuration (the global minimum) and the less favorable configuration (probably a saddle point) is directly relevant to adsorbate diffusion.

Previous theoretical studies employing cluster models also determined the preferred bonding sites of Br on the Ag(100) and Au(100) surfaces, as mentioned in Sec. I. *Ab initio* HF calculations showed that Br would prefer to bond at the B_2 site on the Ag(100) surface (by 370 meV/adatom over the H_4 site, and by 570 meV/adatom over the T_1 site).¹⁹ This is inconsistent with both our DFT-supercell calculations and the experimental data.¹⁻⁴ DFT cluster calculations predicted that the binding energy of Br at the H_4 site on both the Ag(100) and Au(100) surfaces was larger than at the B_2 and T_1 sites by 120 meV for Ag(100) [89 meV for Au(100)] and

TABLE II. Total energy differences (in eV per unit cell) between different configurations of the Br/Ag(100)- $c(2 \times 2)$ and Br/Au(100)- $c(2 \times 2)$ surfaces, obtained from calculations with supercells containing a 9-layer slab and a 7-layer vacuum region, a cutoff energy of 20 Ry, and 56 special \mathbf{k} -points.

$E_{H_4} - E_{B_2}$ (Br/Ag(100))	-0.213
$E_{H_4} - E_{T_1}$ (Br/Ag(100))	-0.557
$E_{B_2} - E_{T_1}$ (Br/Ag(100))	-0.344
$E_{H_4} - E_{B_2}$ (Br/Au(100))	+0.058
$E_{H_4} - E_{T_1}$ (Br/Au(100))	-0.244
$E_{B_2} - E_{T_1}$ (Br/Au(100))	-0.302

202 meV for Ag(100) [202 prefers to bond at the H_4 site on the Au(100) surface is in disagreement with experimental measurements,⁶⁻¹² as well as with our results. We believe that the main problem is that these previous calculations were limited to small clusters, containing only up to 13 metal atoms. It is well known that a small metal cluster has a very different electronic structure than an extended metal surface, yielding very significant differences in adsorbate binding energies and reaction pathways.⁴⁷⁻⁵⁰ Large clusters or extended surface models (e.g., supercell models) are therefore needed to simulate real metal surfaces accurately.

The structural parameters of the optimized geometries for the H_4 , B_2 , and T_1 configurations of the Br/Ag(100) and Br/Au(100) surfaces are presented in Table III. The vertical distances (d_z) between the Br centers and the plane of the centers of the top-layer atoms were calculated to be 1.91 Å on the Ag(100) surface and 2.01 Å on the Au(100) surface for the H_4 structure, 2.16 Å on Ag(100) and 2.18 Å on Au(100) for the B_2 configuration, and 2.48 Å on Ag(100) and 2.46 Å on Au(100) for the T_1 structure. While the values of d_z for the B_2 and T_1 configurations of the Br/Ag(100) surface are very close to the corresponding values for the Br/Au(100) surface, the distance between Br and the surface in the H_4 configuration is observed to be significantly longer (by 0.1 Å) on Br/Au(100) than on Br/Ag(100). Accurate *in-situ* XAFS measurements for Br/Ag(100) in NaBr solution by Endo *et al.* showed that the bond length between Br and its four nearest-neighbor Ag atoms in the H_4 configuration is 2.82 ± 0.05 Å, and the distance between the Br and the surface is 1.94 ± 0.07 Å.⁴ Our results (2.82 Å and 1.91 Å, respectively) are thus in excellent agreement with the experimental data, provided that the solution has only a minor influence on the bond lengths between the adsorbate and the surface.

The bond lengths between Br and Ag and Au clusters of varying size have been obtained with both HF and DFT calculations. Illas *et al.*, using the HF method with a cluster of 5 Ag atoms simulating the H_4 configuration of the Ag(100) surface, obtained a value of 3.43 Å for the length of the Br-Ag bond.²⁰ Paccioni, also using the HF method with slightly larger clusters, found that the bond lengths between a Br ion and the surface Ag atom were 3.24 Å, 2.97 Å, and 2.94 Å in clusters of Br⁻-Ag₁₃ (modeling the H_4 structure), Br⁻-Ag₈ (simulating the B_2 geometry), and Br⁻-Ag₁₃ (representing the T_1 configuration), respectively. Ignaczak and Gomes performed DFT calculations with clusters containing a Br ion and 12 metal atoms and determined the bond lengths to be 3.2 Å, 3.0 Å, and 2.9 Å for the H_4 , B_2 , and T_1 configurations of Br⁻-Ag₁₂ and Br⁻-Au₁₂ clusters, respectively. All of these values are much larger than those obtained from our supercell calculations and the XAFS measurements, suggesting that small clusters do not represent the metal surfaces properly.

The B_2 configuration of the Br/Ag(100) surface shows a very similar relaxation of the surface metal layers as

that of the same configuration for the Br/Au(100) surface. Both undergo an inward relaxation of the top layer and slight outward relaxations of the second and third layers. Similar relaxed structures are also found for the clean Ag(100) and Au(100) surfaces (see Table I).

Our calculations show that the second metal layer undergoes a small buckling with the adsorption of Br in the H_4 configurations. The atoms in the second layer that are immediately below the H_4 sites are observed to shift slightly up towards the surface, while the other atoms in that layer shift up by only on the order of 0.001 Å and hence essentially keep their bulk positions. The spacing between these two sub-layers is found to be 0.02 Å and 0.04 Å for the Br/Ag(100) and Br/Au(100) surfaces. The distance between Br and the second-layer metal atom just below it is still far larger than the bond length between Br and its nearest-neighbor metal atoms in the top layer. Thus a pseudo-five-fold coordination, which has been observed in $c(2 \times 2)$ overlayer structures on bcc metal surfaces,^{51,52} does not exist for the Br/Ag(100) and Br/Au(100) surfaces. This buckling may give rise to an effective Br-Br interaction, mediated through the surface strain field. The top metal layer in the H_4 configurations still shows a slight inward relaxation, similar to the cases of the clean surfaces and the B_2 configurations.

The top metal layer of the T_1 configuration of the Br/Au(100) surface also shows a small buckling. The Au atoms in the top layer that are bonded to Br are observed to undergo a larger inward relaxation than the other half of the Au atoms in the top metal layer. The corresponding buckling is, however, very large for the T_1 configuration of the Br/Ag(100) surface. The distance between the two sublayers formed from the top Ag layer is 0.75 Å, indicating a zigzag surface reconstruction.

Finally, in Table IV we show results of convergence checks for the total-energy differences. Such checks are particularly important for the Br/Au(100) surface due to the small value of the total-energy difference between the H_4 and B_2 configurations. Calculations with a higher cutoff energy (30 Ry) obtained total-energy differences within 1 meV of those from calculations with a cutoff energy of 20 Ry. Increasing the number of special \mathbf{k} points from 36 to 56, increasing the slab thickness from 7 to 9 metal layers, and increasing the vacuum region in the supercell from 5 to 7 layers, all changed the results by only a few meV. Supercells with 5 metal layers are seen to cause errors in the total-energy differences of ~ 30 meV for Br/Ag(100) and ~ 10 meV for Br/Au(100). The use of 20 special \mathbf{k} points also causes an error of ~ 10 meV. Therefore, it is necessary to employ supercells with at least 7 metal layers and 36 special \mathbf{k} points for obtaining the total-energy differences with errors smaller than 10 meV. The distances between Br and its nearest-neighbor metal atoms were also checked. We found that the changes of these distances were smaller than 0.01 Å over the ranges of cut-off energies between 20 and 30 Ry, numbers of \mathbf{k} points between 20 and 56, and numbers of metal layers between 5 and 9 in the supercells, indicating

that the bond lengths are not very sensitive to the choice of computational parameters.

2. Electronic properties and bonding character

In order to better understand the differences between the bonding of bromine on the Ag(100) and Au(100) surfaces, we calculated the total electronic density of states (DOS), the DOS projected onto individual atoms and specific atomic states, and the charge transfer between bromine and the substrate.

Figure 2 shows the total DOS for the Br-adsorbed Ag(100) and Au(100) surfaces. For comparison, the total DOS for the clean relaxed Ag(100) and Au(100) surfaces are also shown. The peaks of the DOS curves for the clean surfaces represent the main features of the s and d states of the substrates and remain essentially at the same positions when bromine atoms are adsorbed. New states are, however, found to be located at between -15 eV and -13 eV relative to the Fermi level in the DOS curves of the Br-adsorbed Ag(100) and Au(100) surfaces. These states are predominantly the bromine $3s$ states with small contributions from the s and d states of the substrate, as seen from the curves for the DOS projected onto the specific atomic states of the adsorbate and the substrate (shown in Fig. 3). Significant changes of the total DOS in the higher energy range close to the Fermi level (above -2.5 eV and -1.5 eV for the Br/Ag(100) and the Br/Au(100) surfaces, respectively) are also observed

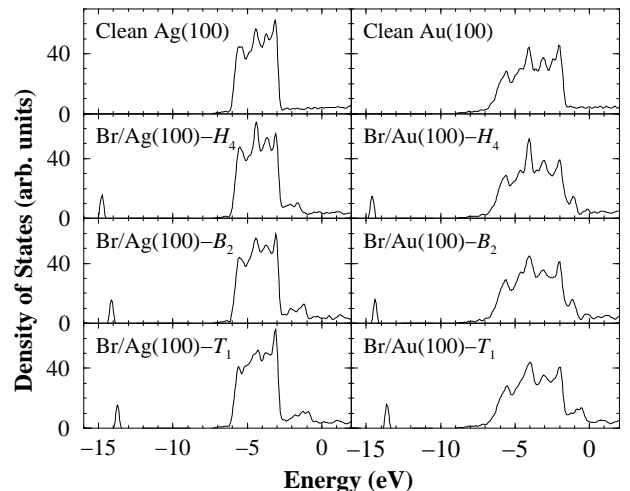


FIG. 2. Total density of states for the clean relaxed and the Br-adsorbed Ag(100) and Au(100) surfaces. The Fermi level is at 0 eV. In this figure, as well as in Figs. 3 and 4, the curves are obtained from calculations with supercells containing a 7-layer slab and a 7-layer vacuum region, a cutoff energy of 20 Ry, and 36 special \mathbf{k} -points.

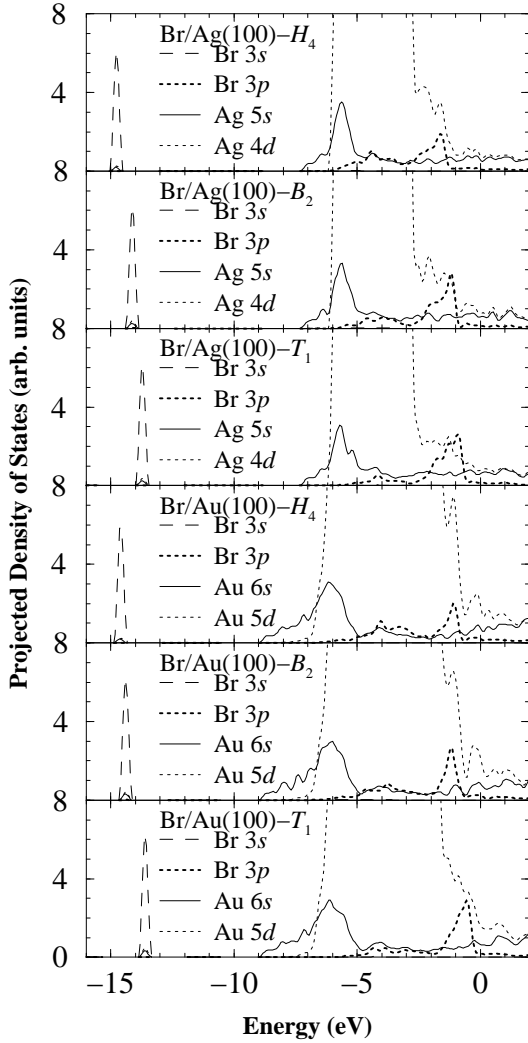


FIG. 3. The density of states projected onto the Br $3s$, Br $3p$, Ag $5s$, Ag $4d$, Au $6s$, and Au $5d$ states for the H_4 , B_2 , and T_1 configurations of the Br-adsorbed Ag(100) and Au(100) surfaces.

when the DOS curves for the clean surfaces are compared with those for the H_4 , B_2 , and T_1 configurations of the Br-adsorbed surfaces (see Fig. 2). The electronic states in the higher energy range are composed mostly of the bromine $3p$ states and the Ag $4d$ (or Au $5d$) states, with some contributions coming from the Ag $5s$ (or Au $6s$) states (see Fig. 3).

In Fig. 4, we show the DOS projected onto bromine for the systems before and after adsorption. The results for the systems before adsorption were calculated by employing the supercell of a 7-layer slab and a 7-layer vacuum region. A bromine layer with a $c(2 \times 2)$ periodicity was kept fixed in the middle of the vacuum region (located at ~ 7 Å above the surface) so that there was essentially no interaction between Br and the substrate. The peaks located in the lower and higher energy ranges in the projected DOS before adsorption are due to the Br

$3s$ and $3p$ states, respectively. The slight broadening of the $3p$ states reflects the weak $3p$ - $3p$ interaction between neighboring bromine atoms. When bromine is adsorbed, both the $3s$ and $3p$ states shift down in energy due to the bonding between bromine and the substrate. A broadening of the Br $3p$ states is also observed and can be attributed to the hybridization of the bromine $3p$ states with the s - and d -bands of the substrates (see Fig. 3). The Br $3s$ states are also seen to mix slightly with the s and d states of the substrate (see also Fig. 3). The hybridization of the Br $3s$ and $3p$ states with the electronic states of the substrate suggests covalent bonding between bromine and the Ag(100) and Au(100) surfaces.

The bonding of Br with the Ag(100) and Au(100) surfaces is also found to be associated with a charge transfer from the substrate to Br. To obtain a rough estimate of the charge transfer, we calculated the change of the charge for a bromine atom upon adsorption by integrating the difference of the corresponding charge densities over a sphere with a radius of 1.28 Å around the atom.⁵³ We found that 0.15 and 0.14 electrons were transferred from the Ag(100) and Au(100) surfaces, respectively, to the bromine atom. The amount of the charge transfer was found to be basically the same for the H_4 , B_2 , and T_1 configurations. These results are consistent with the data for the DOS projected onto the Br atom. By integrating the $3p$ contributions up to the Fermi level, we observe that more $3p$ states are occupied in the Br-adsorbed surfaces than in the systems before adsorption (see Fig. 4). A recent periodic GGA calculation with a local basis set for the adsorption of chlorine on the Ag(111) surface also found that a slight charge (~ 0.2 electrons) was transferred from the Ag(111) substrate to the chlorine atom.⁵⁴ Experimental measurements of the electroadsorption valency of Br adsorbed on Ag(100) report values of approximately -0.70 to -0.75 ,^{5,13,15,16} corresponding to a residual charge of 0.25 to 0.30 electrons on the adsorbed Br. These values are considerably larger than our calculated charge of 0.15 electrons. The discrepancy may be due to the fact that our calculations were performed for systems in vacuum. In an electrochemical environment, the net charge associated with the adsorbate might be very different from that in vacuum, due to solvation. However, the discrepancy might also be attributed to inaccuracies in the theoretical and experimental methods used to estimate the charge.

The difference in the bonding strength of the bromine with the substrate between the different configurations directly affects their relative stability. Based on our DOS data, we provide a qualitative explanation of the difference in bonding strength between the H_4 and B_2 configurations. The Br $3s$ and $3p$ states in the Br/Ag(100)- H_4 configuration are significantly lower in energy than in the Br/Ag(100)- B_2 configuration (see Fig. 4). In addition, the intensity of the lower part of the $3p$ states (below approximately -3 eV) is larger for Br/Ag(100)- H_4 than for Br/Ag(100)- B_2 . Both facts suggest a stronger bonding for the H_4 configuration on Ag(100). This is expected

since there are more direct bonding neighbors for the bromine atom at the H_4 site. On the other hand, the Br

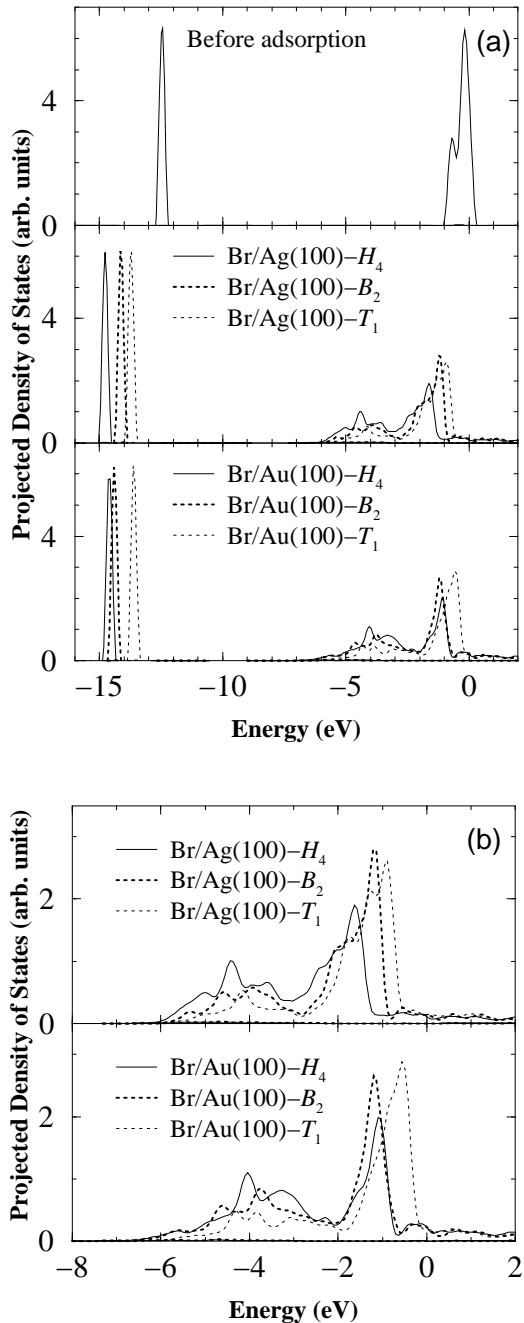


FIG. 4. The density of states projected onto Br for the H_4 , B_2 , and T_1 configurations of the Br-adsorbed Ag(100) and Au(100) surfaces (a) over a larger energy range (-16 eV to 2 eV) in which both the $3s$ and $3p$ states are shown, and (b) over a smaller energy range (-8 eV to 2 eV) where only the $3p$ states are presented. Also shown in (a) is the DOS projected onto Br without adsorption.

$3s$ states in the Br/Au(100)- H_4 configuration are only slightly lower in energy than in the Br/Au(100)- B_2 configuration. While the Br $3p$ states extend over almost the same range in energy for the Br/Au(100)- H_4 and - B_2 configurations, they have slightly larger intensity in the lower part (below ~ -2 eV) and smaller intensity in the higher part (above ~ -2 eV) for the Br/Au(100)- H_4 configuration than for the Br/Au(100)- B_2 configuration. While the H_4 configuration thus has a stronger covalent bonding for both the Br-adsorbed Ag(100) and Au(100) surfaces, the difference in bonding strength between the H_4 and the corresponding B_2 configurations is smaller for the Au(100) surface than for the Ag(100) surface. This is probably due to the fact that the Au $6s$ and $5d$ electrons are more delocalized than the Ag $5s$ and $4d$ electrons, and the bonding strength is expected to be less sensitive to the bonding sites for substrates with more delocalized electrons. In addition to the stronger covalent bonding, the Coulomb attraction resulting from the charge transfer in the H_4 configuration is also stronger than the corresponding B_2 configuration for both the Br/Ag(100) and Br/Au(100) systems, due to the shorter distance between bromine and the surface in the H_4 configuration (see Table III).

It is clear that there is a delicate competition between the attractive and repulsive interactions in each configuration. In particular, the core-core repulsion between bromine and the substrate, which is irrelevant to the electronic DOS but makes a contribution to the total energy of the system, in the H_4 configuration is stronger than in the B_2 configuration. The core-core repulsive energy is calculated as an Ewald sum^{28,55} (see the third column of Table V). The total energy, as determined in our DFT calculations, contains as separate parts the electronic and the core-core Coulomb contributions. Differences of the electronic and the core-core contributions to the total energy between the H_4 and the B_2 configuration are presented in Table V. We note that consideration of the electronic contributions alone does not properly address the opposite order of the total-energy difference (ie, the binding-energy difference) between the H_4 and B_2 configurations for the the Br/Ag(100) and Br/Au(100) surfaces. The core-core interactions need to be included. For both the Br/Ag(100) and Br/Au(100) surfaces, the electronic contribution favors the H_4 configuration, while the core-core contribution favors the B_2 configuration. In the Ag(100) case, the core-core energy, which is higher for H_4 than for B_2 , is more than compensated by the lower electronic energy for the H_4 configuration, resulting in H_4 being the preferred bonding site for Br on Ag(100). For the Br/Au(100) system, however, the lower electronic energy for the H_4 configuration only partially compensates the higher core-core energy for Br/Au(100)- H_4 . As a result, the B_2 configuration is lower in total energy than the H_4 configuration for the Br-adsorbed Au(100) surface. The small magnitudes of the total-energy differences, compared to the individual electronic and core-core contributions, strongly empha-

size the need for very accurate energy calculations and careful convergence checks.

IV. CONCLUSIONS

The theoretical approach of supercell models combined with first-principles total-energy DFT pseudopotential methods has reproduced experimental measurements of preferred adsorption sites for Br-chemisorbed Ag(100) and Au(100) surfaces.

We have shown that while the hollow-site configuration is more stable on the Br/Ag(100) surface (by 210 meV/adatom over the bridge-site structure), the bridge-site configuration is more stable than the corresponding hollow-site structure by 60 meV/adatom on the Br/Au(100) surface. The calculations also predict that the one-fold on-top configuration is the least stable structure on both surfaces (560 meV and 300 meV higher than the corresponding most stable structure for the Br/Ag(100) and Br/Au(100) surfaces, respectively). Other aspects of the geometries of the Br/Ag(100) and Br/Au(100) systems have also been determined and are shown to be in excellent agreement with the available experimental data.

The bond between Br and the substrate is found to be covalent with a slight polarization due to a small charge transfer from the substrate to the bromine. The chemical bonding between Br and the substrate is shown to be stronger in the H_4 configuration than in the B_2 configuration. Compared with the Br/Ag(100) surface, however, the Br/Au(100) surface exhibits a reduced difference in the bonding strength between the H_4 and B_2 configurations. The core-core Coulomb interaction is found to be higher for the H_4 configuration than for the B_2 configuration. The detailed balance between the electronic and the core-core contributions to the total energy determines H_4 and B_2 as the preferred bonding site on the Ag(100) and Au(100) surfaces, respectively.

Our work demonstrates that the use of extended surface models and careful convergence checks are critical for obtaining reliable information on the Br/Ag(100) and Br/Au(100) systems from *ab initio* calculations.

ACKNOWLEDGMENTS

We thank S. J. Mitchell and L. G. Wang for helpful discussions. We also thank S. P. Lewis, M. A. Novotny and G. Brown for comments on the manuscript. This work was supported by the National Science Foundation under grant No. DMR-9981815 and by Florida State University through the Center for Materials Research and Technology and the School of Computational Science and Technology.

- ¹ K. K. Kleinherbers, E. Janssen, A. Goldmann, and H. Saalfeld, *Surf. Sci.* **215**, 394 (1989).
- ² B. M. Ocko, J. X. Wang, and Th. Wandlowski, *Phys. Rev. Lett.* **79**, 1511 (1997).
- ³ C. Hanewinkel, A. Otto, and Th. Wandlowski, *Surf. Sci.* **429**, 255 (1999).
- ⁴ O. Endo, M. Kiguchi, T. Yokoyama, M. Ito, and T. Ohta, *J. Electroanal. Chem.* **473**, 19 (1999).
- ⁵ Th. Wandlowski, J. X. Wang, and B. M. Ocko, *J. Electroanal. Chem.* **500**, 418 (2001).
- ⁶ E. Bertel and F. P. Netzer, *Surf. Sci.* **97**, 409 (1980).
- ⁷ F. P. Netzer, E. Bertel, and J. A. D. Matthew, *Solid State Commun.* **33**, 519 (1980).
- ⁸ B. M. Ocko, O. M. Magnussen, J. X. Wang, and Th. Wandlowski, *Phys. Rev. B* **53**, R7654 (1996).
- ⁹ Th. Wandlowski, J. X. Wang, O. M. Magnussen, and B. M. Ocko, *J. Phys. Chem.* **100**, 10277 (1996).
- ¹⁰ T. Pajkossy, T. Wandlowski, and D. M. Kolb, *J. Electroanal. Chem.* **414**, 209 (1996).
- ¹¹ B. M. Ocko, O. M. Magnussen, J. X. Wang, R. R. Adzic, and Th. Wandlowski, *Physica B* **221**, 238 (1996).
- ¹² A. Cuesta and D. M. Kolb, *Surf. Sci.* **465**, 310 (2000).
- ¹³ M. T. M. Koper, *J. Electroanal. Chem.* **450**, 189 (1998).
- ¹⁴ M. T. M. Koper, *Electrochim. Acta* **44**, 1207 (1998).
- ¹⁵ S. J. Mitchell, G. Brown, and P. A. Rikvold, *J. Electroanal. Chem.* **493**, 68 (2000).
- ¹⁶ S. J. Mitchell, G. Brown, and P. A. Rikvold, *Surf. Sci.* **471**, 125 (2001).
- ¹⁷ J. A. N. F. Gomes and A. Ignaczak, *J. Mol. Struct. (Theochem.)* **463**, 113 (1999).
- ¹⁸ A. Ignaczak and J. A. N. F. Gomes, *J. Electroanal. Chem.* **420**, 71 (1997).
- ¹⁹ G. Pacchioni, *Electrochim. Acta* **41**, 2285 (1996).
- ²⁰ F. Illas, J. Rubio, J. M. Ricart, and J. A. Garrido, *J. Electroanal. Chem.* **200**, 47 (1986).
- ²¹ G. Kresse and J. Hafner, *Phys. Rev. B* **47**, 558 (1993).
- ²² G. Kresse and J. Furthmüller, *Comput. Mat. Sci.* **6**, 15 (1996).
- ²³ G. Kresse and J. Furthmüller, *Phys. Rev. B* **54**, 11169 (1996).
- ²⁴ J. P. Perdew, J. A. Chevary, S. H. Vosko, K. A. Jackson, M. R. Pederson, D. J. Singh, and C. Fiolhais, *Phys. Rev. B* **46**, 6671 (1992).
- ²⁵ J. P. Perdew and Y. Wang, *Phys. Rev. B* **45**, 13244 (1992).
- ²⁶ D. Vanderbilt, *Phys. Rev. B* **41**, 7892 (1990).
- ²⁷ G. Kresse and J. Hafner, *J. Phys.: Condens. Matter* **6**, 8245 (1994).
- ²⁸ M. C. Payne, M. P. Teter, D. C. Allan, T. A. Arias, and J. D. Joannopoulos, *Rev. Mod. Phys.* **64**, 1045 (1992).
- ²⁹ CRC, *CRC Handbook of Chemistry and Physics*, 77th edn. (CRC press, Boca Raton, 1996).
- ³⁰ A. Khein, D. J. Singh, and C. J. Umrigar, *Phys. Rev. B* **51**, 4105 (1995).
- ³¹ B. D. Yu and M. Scheffler, *Phys. Rev. Lett.* **77**, 1095 (1996); *Phys. Rev. B* **55**, 13916 (1997).
- ³² C. Ratsch, A. P. Seitsonen, and M. Scheffler, *Phys. Rev. B* **55**, 6750 (1997).
- ³³ P. A. Gravi, D. M. Bird, and J. A. White, *Phys. Rev. Lett.* **77**, 3933 (1996).
- ³⁴ P. A. Gravi, J. A. White, and D. M. Bird, *Surf. Sci.* **352**,

- 248 (1996).
- ³⁵ A. Eichler, G. Kresse, and J. Hafner, *Surf. Sci.* **397**, 116 (1998).
- ³⁶ M. Asato, A. Settels, T. Hoshino, T. Asada, S. Blügel, R. Zeller, and P. H. Dederichs *Phys. Rev. B* **60**, 5202 (1999).
- ³⁷ L. Vitos, A. V. Ruban, H. L. Skriver, and J. Kollár, *Surf. Sci.* **411**, 186 (1998).
- ³⁸ B. D. Yu and M. Scheffler, *Phys. Rev. B* **56**, R15569 (1997).
- ³⁹ M. Methfessel, D. Hennig, and M. Scheffler, *Phys. Rev. B* **46**, 4816 (1992).
- ⁴⁰ G. Boisvert, L. J. Lewis, M. J. Puska, R. M. Nieminen, *Phys. Rev. B* **52**, 9078 (1995).
- ⁴¹ V. Fiorentini, M. Methfessel, and M. Scheffler, *Phys. Rev. Lett.* **71**, 1051 (1993).
- ⁴² M. Weinert, R. E. Watson, J. W. Davenport, and G. W. Fernando, *Phys. Rev. B* **39**, 12585 (1989).
- ⁴³ H. Erschbaumer, A. J. Freeman, C. L. Fu, and R. Podloucky, *Surf. Sci.* **243**, 317 (1991).
- ⁴⁴ R. Eibler, H. Erschbaumer, C. Temnitschka, R. Podloucky, and A. J. Freeman, *Surf. Sci.* **280**, 398 (1993).
- ⁴⁵ K. P. Bohnen and K. M. Ho, *Vacuum* **41**, 416 (1990).
- ⁴⁶ H. Li, J. Quinn, Y. S. Li, D. Tian, F. Jona, and P. M. Marcus, *Phys. Rev. B* **43**, 7305 (1991).
- ⁴⁷ J. L. Whitten and H. Yang, *Surf. Sci. Rep.* **24**, 55 (1996).
- ⁴⁸ I. Panas, P. E. M. Siegbahn, and U. Wahlgren, *Chem. Phys.* **112**, 325 (1987).
- ⁴⁹ R. L. Whetten, D. M. Cox, D. J. Trevor, and A. Kaldor, *Phys. Rev. Lett.* **54**, 1494 (1985).
- ⁵⁰ M. D. Mores, M. E. Gensic, J. R. Heath, and R. E. Smalley, *J. Chem. Phys.* **83**, 2293 (1985).
- ⁵¹ K. Griffiths, D. A. King, G. C. Aers, and J. B. Pendry, *J. Phys. C* **15**, 4921 (1985).
- ⁵² M. P. Bessent, P. Hu, A. Wander, and D. A. King, *Surf. Sci.* **325**, 272 (1995).
- ⁵³ The value of 1.28 Å was chosen to be intermediate between the atomic (1.14 Å) and ionic (1.95 Å) radii of bromine, but closer to the atomic radius.
- ⁵⁴ K. Doll and N. M. Harrison, *Phys. Rev. B* **63**, 165410 (2001).
- ⁵⁵ J. Ihm, A. Zunger, and M. L. Cohen, *J. Phys. C: Solid State Phys.* **12**, 4409 (1979).

TABLE III. Relaxation of the H_4 , B_2 , and T_1 configurations of the Br/Ag(100)- $c(2 \times 2)$ and Br/Au(100)- $c(2 \times 2)$ surfaces. Also shown are the vertical distance (d_z , in units of Å) between Br and the plane of the centers of the top-layer atoms on the surface, and the distance (d , in units of Å) between Br and its nearest-neighbor metal atom(s). The change in spacing between layers i and j is denoted by Δd_{ij} . When sub-layers are present, the changes are denoted by Δd_{ij} and $\Delta d'_{ij}$, with Δd_{ij} being the larger in magnitude. d_0 is the same as in Table I. The computational details are the same as in Table II.

	d_z	d	$\Delta d_{12}/d_0$ (%)	$\Delta d'_{12}/d_0$ (%)	$\Delta d_{23}/d_0$ (%)	$\Delta d'_{23}/d_0$ (%)	$\Delta d_{34}/d_0$ (%)
Br/Ag(100)- H_4	1.91	2.82	-0.6	0.1	0.8	0.1	-0.0
Br/Ag(100)- B_2	2.16	2.61	-0.9		0.5		0.2
Br/Ag(100)- T_1	2.48	2.48	10.4	-7.7	0.2		-0.1
Br/Au(100)- H_4	2.01	2.89	-1.6	0.2	1.4	-0.3	0.4
Br/Au(100)- B_2	2.18	2.62	-0.9		0.4		0.3
Br/Au(100)- T_1	2.46	2.46	-1.2	-0.5	0.5		0.4

TABLE IV. Convergence checks for the total energy differences (in units of eV per unit cell) between different configurations with respect to the cutoff energy (E_{cut} , in units of Ry), the number of metal layers (N_m) in the supercell, the thickness of the vacuum region (N_v , in units of number of bulk metal layers), and the number of \mathbf{k} points in the surface Brillouin zone (N_k).

E_{cut}	N_m	N_v	N_k	$E_{H_4} - E_{B_2}$	$E_{H_4} - E_{T_1}$	$E_{H_4} - E_{B_2}$	$E_{B_2} - E_{T_1}$
				Br/Ag(100)	Br/Ag(100)	Br/Au(100)	Br/Au(100)
20	5	7	20	-0.191	-0.526	+0.061	-0.282
20	7	7	20	-0.222	-0.556	+0.048	-0.285
20	7	7	36	-0.211	-0.552	+0.056	-0.291
30	7	7	36	-0.212	-0.552	+0.057	-0.291
20	7	5	36	-0.210	-0.550	+0.057	-0.289
20	7	7	56	-0.210	-0.551	+0.059	-0.294
20	9	7	56	-0.213	-0.557	+0.058	-0.302

TABLE V. Differences (in eV per unit cell) of two energy contributions to the total energy between the H_4 and B_2 configurations. E^e and E^{cc} are the electronic and core-core Coulomb contributions, respectively. Also shown is the total-energy difference ($E_{H_4}^{tot} - E_{B_2}^{tot}$). The results are obtained from calculations with supercells containing a 7-layer slab and a 7-layer vacuum region, a cutoff energy of 20 Ry, and 36 special \mathbf{k} -points.

	$E_{H_4}^e - E_{B_2}^e$	$E_{H_4}^{cc} - E_{B_2}^{cc}$	$E_{H_4}^{tot} - E_{B_2}^{tot}$
Br/Ag(100)	-429.230	+429.018	-0.212
Br/Au(100)	-371.156	+371.213	+0.057